

Synchronization in coupled cells with activator-inhibitor pathways

S. Rajesh,¹ Sudeshna Sinha,² and Somdata Sinha^{1,*}

¹Centre for Cellular and Molecular Biology, Uppal Road, Hyderabad 500007, India

²The Institute of Mathematical Sciences, CIT Campus, Chennai 600113, India

(Received 5 July 2006; revised manuscript received 16 October 2006; published 9 January 2007)

The functional dynamics exhibited by cell collectives are fascinating examples of robust, synchronized, collective behavior in spatially extended biological systems. To investigate the roles of local cellular dynamics and interaction strength in the spatiotemporal dynamics of cell collectives of different sizes, we study a model system consisting of a ring of coupled cells incorporating a three-step biochemical pathway of regulated activator-inhibitor reactions. The isolated individual cells display very complex dynamics as a result of the nonlinear interactions common in cellular processes. On coupling the cells to nearest neighbors, through diffusion of the pathway end product, the ring of cells yields a host of interesting and unusual dynamical features such as, suppression of chaos, phase synchronization, traveling waves, and intermittency, for varying interaction strengths and system sizes. But robust complete synchronization can be induced in these coupled cells with a small degree of random coupling among them even where regular coupling yielded only intermittent synchronization. Our studies indicate that robustness in synchronized functional dynamics in tissues and cell populations in nature can be ensured by a few transient random connections among the cells. Such connections are being discovered only recently in real cellular systems.

DOI: 10.1103/PhysRevE.75.011906

PACS number(s): 87.18.Hf, 47.54.-r, 05.45.-a

I. INTRODUCTION

A single cell, which is the basic building block of all living organisms, performs its functions through various substrates that are produced by the intracellular network of regulated biochemical reaction pathways. Even though end-product inhibition is the single most common motif of regulation in biochemical pathways, as it ensures homeostasis, a large number of biochemical pathways consist of multiple regulatory loops through positive and negative feedback processes such as, enzyme activation-inhibition, gene induction-repression, etc. [1–3]. The chemical kinetics of these feedback reactions and other intracellular processes involve high order of nonlinearity, and, therefore, these pathways in the cells often show a variety of nonlinear phenomena such as self-sustained oscillations, birhythmicity and chaos [4–6].

In a population and in the multicellular state (e.g., tissues), cells interact with each other directly or indirectly. Hence, the dynamics of an individual cell may be influenced by the interaction or coupling with other cells. Living systems use such interactions to coordinate and control many biological functions [7–11]. There is a diversity of coupling mechanisms that nature uses to enforce communication among cells in a cellular ensemble. In biological tissues, the arrangement and types of contacts complement their specific functions. Such intercellular signaling couples the biochemical reaction pathways within each cell through diffusion of the products of these reactions. Such diffusive coupling occurs in metabolically coupled cells, which leads to robust synchrony among cells and spatial patterns in cellular ensembles [12–14].

In reality, a small degree of randomness in spatial coupling can be expected to exist along with the strict nearest

neighbor scenarios discussed above. Indeed, many systems of biological, technological, and physical significance are better described by randomizing some fraction of the regular links [15], as it allows information to be transferred at longer distances in lesser time. Recently a diversity of interactions have been shown to enforce communication among spatially non-neighboring cells. Recent experimental demonstrations of mechanisms of transient long distance interactions through substrates or cellular processes (“nanotubes”), are shown to regulate multicellular functions [16]. It is not clearly understood how the local functional dynamics of each cell, the features of intercellular signaling, and the system size interact to ensure that robustness and regulative capacity emerges at the tissue or population level.

The most interesting feature of the coupled system is its global behavior under different dynamic conditions of its constituent cells. The two most important emergent behaviors in coupled systems are—synchrony and spatiotemporal patterns [17]. Synchronization is a phenomena that widely occurs in coupled nonlinear systems. Natural systems as diverse as clocks, flashing fireflies, cardiac pacemakers and firing neurons exhibit a tendency to operate in synchrony. One can have synchronization of a periodic oscillator by external force, or the well-known phenomena of phase locking and frequency entrainment of periodic oscillators. Interestingly, chaotic systems, though much more complex, also synchronize in varying degrees, such as (i) *complete synchronization* (CS) where the difference between signals virtually disappears [18]; (ii) *lag synchronization* (LS) where the subsystems are synchronized with a delay or time shift [19]; (iii) *generalized synchronization* (GS) where the instantaneous states of subsystems are interrelated by a functional dependence [20]; (iv) *phase synchronization* (PS) where the systems remain largely uncorrelated, but the mean time scales of their oscillations coincide or become commensurate [21], i.e., the phases of the systems are locked even though the amplitudes may be uncorrelated; and (v) *intermittent*

*Electronic address: sinha@ccmb.res.in

phase synchronization (IPS) where the phase entrainment is lost and regained intermittently [22].

Phase synchronization is the weakest form of synchronization and is observed typically when coupling is weak. As coupling strengths increase more ordered stages of synchronized dynamics are obtained, such as lag synchronization followed by the strongest synchronization, the complete synchronization [17]. It has also been observed that at the onset of these kinds of synchronization, at the thresholds of coupling strengths, one obtains intermittent behavior (such as IPS). This intermittency precedes regular synchronized dynamics and is characterized by epochs of synchronization interrupted by intervals of loss of synchronization. In biological systems, it is hard to find two exactly identical systems, and hence phase synchronization is more natural compared to the complete synchronization. Thus, the concept of phase synchronization has been applied for the study of synchrony in many biological processes [23].

In this paper we have studied a model cell-collective—a ring of coupled cells, each incorporating a three-step model biochemical network, that involves a positive and a negative feedback process. The pathway reactions are of the activator-inhibitor type, which have commonly been found underlying pattern forming mechanisms in tissues and organisms [24–28]. The coupling among the cells are diffusive through the end product of the pathway to their nearest neighbors in the lattice. We choose parameter regimes where the local dynamics of the pathways are chaotic in the uncoupled cells [29]. We have analyzed the collective behavior of the ring of cells on coupling, with the aim to investigate the role of coupling strength and type (i.e., local or transient long distance), and system size (i.e., the number of cells).

We observe that this coupled cell system does not follow any predicted route of synchronization with system size and coupling strength as discussed earlier. It shows complete chaotic synchronization for all coupling strengths only in the case of small lattice sizes. Mostly it shows intermittency for weak and very high levels of coupling for medium and larger lattices. For a narrow range of medium lattice sizes, it shows complete suppression of chaos to higher periodic (P4) oscillations, and spatiotemporal patterns, including chaotic traveling waves for a number of initial conditions, for a small range of coupling strengths. The coexistence of lower subharmonic oscillations with constant phase slips is a new kind of standing wave pattern observed in this coupled cell model. Though intermittency is the primary dynamical behavior exhibited by this ring of cells, we also demonstrate that the introduction of a few transient nonlocal connections between the cells can have a dramatic effect on synchronizing the cells dynamics for a large range of coupling strength and system sizes. This has important implications in synchronization of functional dynamics in cell ensembles under widely different conditions. This also argues against the requirement of strict conditions for robust synchronized activity in tissues and multicell systems, which is unrealistic in natural or experimental conditions.

II. MODELS AND METHOD

A. Single cell model

The model single cell incorporates a representative biochemical pathway that is regulated by negative and positive

feedback processes. It is a three-step activator-inhibitor reaction sequence regulated by the end product through two feedback loops—end-product inhibition of the first substrate, and autocatalytic activation, through an allosteric enzyme-mediated reaction, of the end product. The abundance of negative feedback control in biochemical reaction pathways helps maintaining homeostasis in cellular functions by suppressing stochastic variations [30], and thereby provides the required robustness in cellular functions. Though less prevalent, positive feedback processes in both metabolic and genetic regulations are used for important activities through amplification of signals, rapid response pathways, “switching” activities, and in cellular processes that show periodic and complex dynamics, such as glycolytic oscillations in cell free extracts of yeast cells, peroxidase-oxidase reactions, insulin secretion in pancreatic beta cells, calcium oscillations, and amplification of cAMP signal in the aggregation of cellular slime molds [4,31]. Thus we consider this three-step model pathway to be a simple and general scheme that may represent a large variety of functional dynamics observed in cellular systems. The details of the model are given in Ref. [32].

The change in the concentrations of the three substrates in this reaction pathway can be described by the following equations:

$$\begin{aligned}\frac{dx}{dt} &= F(z) - kx, \\ \frac{dy}{dt} &= x - G(y,z), \\ \frac{dz}{dt} &= G(y,z) - qz,\end{aligned}\tag{1}$$

where x , y , and z are the normalized concentrations of the substrates, and k and q are the rates of degradation of the first substrate and end product, respectively, which follow first order kinetics and are nonsaturated. The functions $F(z)$ and $G(y,z)$ represent the negative and positive feedback processes (viz. end-product inhibition and the autocatalytic activation), which are nonlinear kinetic processes. The molecular interactions for such biochemical regulations are modeled using reactions that are widespread in both genetic and metabolic reactions underlying cellular processes, such as, the cell cycle, gene repression-induction, glycolysis, hormonal signaling, cAMP oscillations in cellular slime molds, calcium-induced-calcium-release (CICR), etc. [4,33]. These are given by

$$F(z) = \frac{1}{1+z^4}, \quad G(y,z) = \frac{Ty(1+y)(1+z)^2}{L+(1+y)^2(1+z)^2},\tag{2}$$

where, L and T are related to the allosteric constant and maximum velocity of the enzyme.

The parameter values used in this model pathway are chosen keeping in mind the following pathways incorporating positive and negative feedback processes—cell cycle, glycolytic cycle, and cAMP oscillations in slime molds [1,34]. The normal parameter values in this pathway are $L=10^6$, $T=10$,

$k=1$, and $q=0.01$, where it shows simple limit cycle oscillations. The dynamics exhibited by this pathway is a function of the parameters [29,35]. The orders of magnitude of the three variables are quite different as a small variation in x leads to large variations in y and z due to the autocatalytic effect, even though, due to the negative feedback, this large variation is suppressed to smaller amplitude oscillations in x . The temporal variation of the end-product z , being of primary interest, is displayed in all figures.

B. Coupled cell model

The model single cells [Eq. (1)], are coupled with their two nearest neighbors by the diffusion of the end product of their respective activator-inhibitor reaction pathways, on a one-dimensional lattice with periodic boundary conditions [36,37]. The coupled-cell model can be written as

$$\frac{dx_i}{dt} = F(z_i) - kx_i,$$

$$\frac{dy_i}{dt} = x_i - G(y_i, z_i),$$

$$\frac{dz_i}{dt} = G(y_i, z_i) - qz_i - \epsilon z_i + \frac{\epsilon}{2}(z_{i-1} + z_{i+1}), \quad (3)$$

where, ϵ is the diffusive coupling strength of the end product, and, i , the cell number that ranges from 1 to N , where N is the lattice size. For numerical simulation we have used the discretization scheme of Oono and Puri [38], and the fourth-order Runge-Kutta scheme. Simulations have been performed on lattices with varying number of cells, with random initial conditions uniformly distributed around the steady state ($z^* \pm 2, z^* \sim 5.163$). Simulations have been performed for $t \sim 10^5$, and results are presented for the last 5000 time units.

III. RESULTS

A. Single cell dynamics

The biochemical pathway [Eq. (1)] in the single cell exhibits a wide range of dynamics—equilibrium, limit cycle, period-doubling, birhythmic, complex, and chaotic—depending on the values of parameters and initial conditions [29]. For parameters $k=0.003$, $q=0.1$, the pathway exhibits chaotic oscillations. Figure 1 shows various aspects of chaotic behavior in a single cell. The time series of z [Fig. 1(a)] and the (z - y) phase portrait [Fig. 1(c)] clearly show that the oscillations of multiple time scales are associated with the chaotic state of the cell. Earlier studies [29] have shown that there are more than one overlapping attractors that exhibit period-doubling to chaos in this system. The multilayered structure of the return map [Fig. 1(b)], constructed from the successive maxima of z , shows evidence of homoclinic chaos [39]. The power spectrum [Fig. 1(d)] constructed from the time series of z shows a broadband structure with peaks at two major frequencies and also at their higher harmonics. These frequencies ($f_1=0.0114$) and ($f_2=0.0012$) correspond

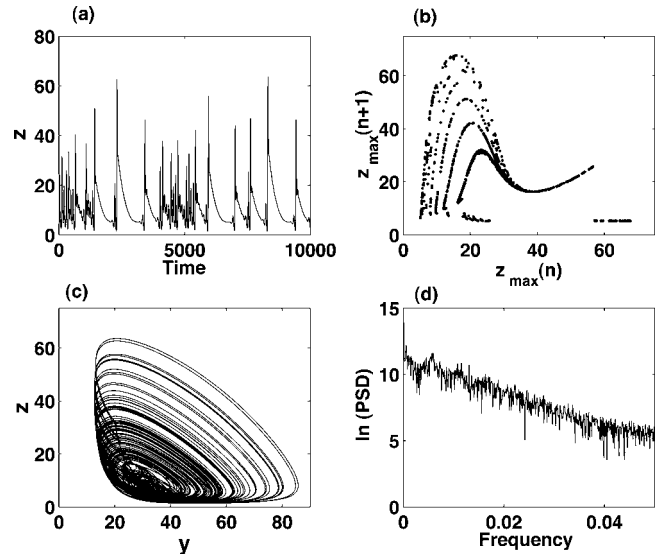


FIG. 1. Single cell dynamics: (a) time series, (b) return map, (c) (y - z) phase portrait, and (d) power spectrum, of z .

to the two different time scales of oscillations associated with the different attractors embedded in the chaotic attractor observed here [35].

Dynamics of uncoupled cells. In a population of similar cells (i.e., having the same parameter values), each cell may differ with each other due to unequal amount of the substrates. The pathway in each cell will be showing chaotic oscillations, and the collective temporal behavior of the uncoupled cells will be a simple superposition of all the cells' behaviors. Figure 2(a) shows the superposition of time series of z in 50 uncoupled cells, where the temporal evolution of the cells' dynamics are totally uncorrelated and the time series are randomly overlapped in the figure. The space-time plot of the end product z in these cells [Fig. 2(b)] shows that each cell continues to synthesize the end product z in a chaotic manner.

B. Dynamics of coupled cells

Two main parameters associated with the coupled system are the total number of cells, N , and the coupling strength, ϵ . Here, we present the results of our study of the collective dynamics of this cell system for different N and ϵ .

1. The role of number of cells (N)

The collective dynamics of cells was studied by varying the number of cells in the ring from $N=10$ to 100 by multiples of 10 for $\epsilon=0.72$. Table I shows the variation of local and global dynamics of the coupled cells with increasing N . The simulations have been done for 10 different initial conditions.

Table I clearly shows that the inclusion of more cells affects the local and global dynamics of the multicellular system. The local behavior of the individual cells remains chaotic (CH), except for $N=50$ where chaos is suppressed to period 4 (P4) dynamics. Thus, under coupling, the local and global dynamics can influence each other depending on the

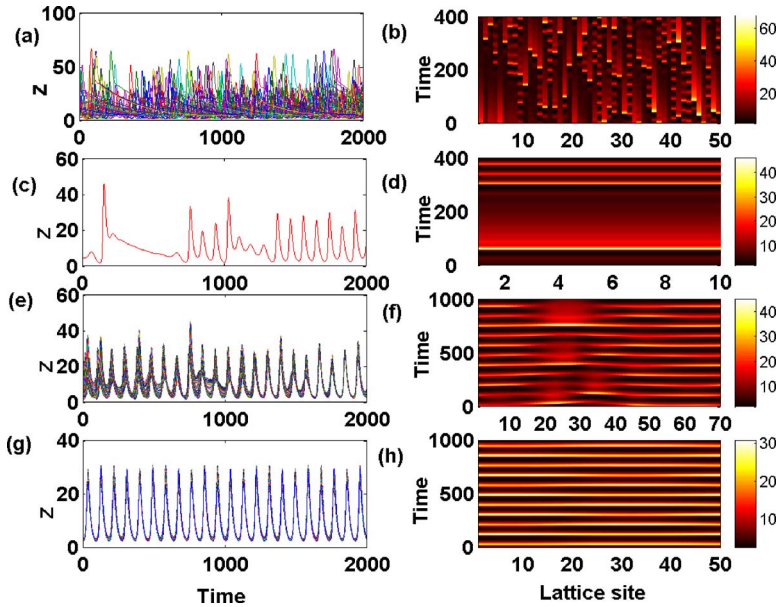


FIG. 2. (Color online) Types of global dynamics shown by the ring of cells of different sizes for $\epsilon=0.72$. Plots in first and second columns represent superposition of time series and the space-time plots of z in all cells. (a, b) $N=50$ uncoupled cells in the lattice; (c, d) complete chaotic synchronization (CS) for $N=10$; (e, f) intermittent phase synchronization (IPS) for $N=70$; and (g, h) suppression of chaos and phase synchronization (PS) for $N=50$.

size of the lattice. The global dynamical states found in the coupled system are complete synchronization (CS), phase synchronization (PS), and primarily intermittent phase synchronization (IPS) (8 out of 10 lattices). Figures 2(c)–2(h) show examples of these different types of global dynamics in lattices of different N .

Small lattices ($N=10, 20$) show complete chaotic synchronization (CS) of dynamics in all cells, and the global dynamics is the same as the local chaotic dynamics [Figs. 2(c) and 2(d)]. The superposition of time series plots of 10 cells gives a single trajectory implying that the end-product concentrations in all cells are moving in exact synchrony on coupling [Fig. 2(c)]. The space-time plot Fig. 2(d) also confirms the perfect synchronization in the lattice. Thus small coupled cell systems can synchronize their dynamics completely to their local chaotic dynamics.

Lattices with increasing N , except for $N=50$, shows intermittent phase synchronization (IPS). This behavior has been seen in larger systems ($N=500$) also. Figures 2(e) and 2(f) illustrate the intermittent behavior of the system for $N=70$. Figure 2(e) shows that the superimposed time series are not exactly overlapping since both phase and amplitude of oscillations in each cell are not perfectly correlated. Figure 2(f) shows that the phase synchrony in the coupled cells is lost for certain intervals of time and is regained within a short span. The loss of phase synchrony appears as the temporary overlap of the peaks in the time series, and local spreads in the space-time plot. Here, the phase synchronized and unsynchronized states form intermittent states, and the system switches between these two states at irregular inter-

vals. This transient loss of synchrony in the lattice continues for very long time. It may be noted here that the local dynamics of all cells remains chaotic.

The lattice with $N=50$ shows local and global dynamics which are very different from that of the uncoupled system [Figs. 2(g) and 2(h)]. Local chaos is suppressed and each cell shows stable period 4 (P4) oscillations. The global dynamics of the cells are found to be phase synchronized with phase slips (discussed later). The time series plots in Fig. 2(g) shows an interesting repeating time course of “two high peaks and two lower peaks” that arise because the peaks of the P4 oscillations in all cells do not overlap at the same time. The space-time plot [Fig. 2(h)] also confirms the relative phase synchrony and periodic nature of the global dynamics.

2. The role of coupling strength (ϵ)

The coupling strength (ϵ) plays an important role in modulating the interaction between the local and global dynamics. We simulated the coupled cell system ($N=50$) for a range of coupling strengths ($0.1 \leq \epsilon \leq 0.9$), and studied their long-term dynamics. It may be recalled that complete synchronization is observed only for small system size. The results are given in Table II.

Table II clearly shows that, except for ($0.7 \leq \epsilon \leq 0.8$), the primary mode of the collective dynamics shown by the lattice is IPS. The other types of dynamics seen for some initial conditions are traveling waves (TW) and periodic phase synchronization (PS+P4). For very small coupling strength ($\epsilon=0.1$), the dynamics is IPS for all initial conditions stud-

TABLE I. Variation of dynamics with cell number, N . Notations: CH, chaos; CS, complete synchronization; P4, period 4 cycle; PS, phase synchronization; IPS, intermittent phase synchronization.

| Number of cells | 10 | 20 | 30 | 40 | 50 | 60 | 70 | 80 | 90 | 100 |
|-----------------|----|----|-----|-----|----|-----|-----|-----|-----|-----|
| Global dynamics | CS | CS | IPS | IPS | PS | IPS | IPS | IPS | IPS | IPS |
| Local dynamics | CH | CH | CH | CH | P4 | CH | CH | CH | CH | CH |

TABLE II. Dynamics of the coupled system ($N=50$) with respect to coupling strength (ϵ), for 50 different initial conditions. The digits indicate the number of initial conditions that go to a particular dynamical state. Notations: IPS+CH is intermittent phase synchronization in the global dynamics while the local dynamics is chaotic; PS+P4 is phase synchronization in the global dynamics while the local dynamics is period 4; TW is the traveling wave regime.

| ϵ | IPS+CH | PS+P4 | TW |
|------------|--------|-------|----|
| 0.1 | 50 | 0 | 0 |
| 0.2 | 49 | 1 | 0 |
| 0.3 | 49 | 0 | 1 |
| 0.4 | 47 | 0 | 1 |
| 0.5 | 48 | 0 | 1 |
| 0.6 | 47 | 0 | 3 |
| 0.7 | 0 | 50 | 0 |
| 0.8 | 8 | 42 | 0 |
| 0.9 | 48 | 2 | 0 |

ied. More cases of PS or TW are observed as the coupling strength increases. For $\epsilon=0.7$, the system only showed period 4 (P4) solution along with phase synchronization. For higher values of coupling strength ($\epsilon=0.8$), the dynamics is primarily periodic though some cases of IPS were observed. Unlike usual cases, for even stronger coupling ($\epsilon=0.9$), the lattice did not remain synchronized, and showed mostly IPS.

Traveling waves (TW) are good examples of spatially nonlocalized structures observed in nonlinear media. Such solutions have been reported earlier in coupled map lattices [40]. For few initial conditions, the traveling wave solutions are also observed in the lattice of size $N=50$ for a range of coupling strength. In Figs. 3(a)–3(d) we present the local and global dynamics of the coupled pathways showing traveling waves for $N=50$, $\epsilon=0.6$. The three-dimensional space-time

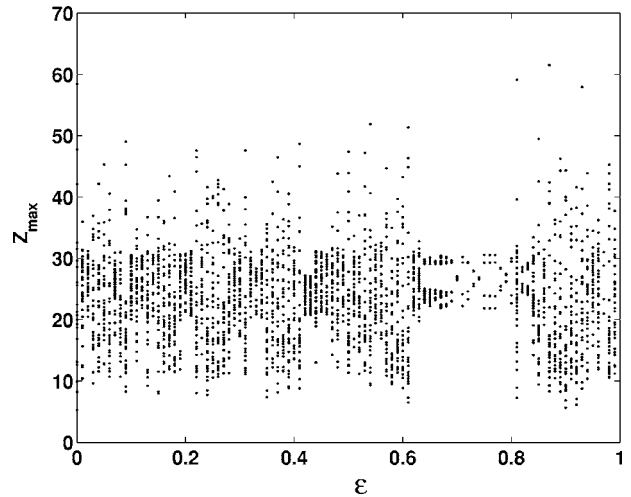


FIG. 4. Plot of z_{\max} of the 25th cell in the lattice ($N=50$) showing variation of long-term local dynamics with increasing ϵ .

plot in Fig. 3(a) shows the traveling wave in z in the lattice. The two-dimensional spatiotemporal evolution of the traveling wave is shown in Fig. 3(b) that shows the phase distribution in the lattice. The peak of the wave travels through the circular lattice with almost uniform velocity. However, the temporal dynamics of the individual cells [Fig. 3(c)] is entirely different from the original attractor [Fig. 1(c)], and the multiple time-scale structure of the original attractor is absent in the new attractor which consists of the small oscillations only [Fig. 3(d)].

Bifurcation diagram, shown in Fig. 4, plots the long term dynamics of (z_{\max}) in the 25th cell for 5000 time points, for different coupling strength. This plot gives an idea about the modulation of the local dynamics due to coupling. The initial conditions have been kept constant for the entire range of coupling strength. It can be seen from the figure that even though for most cases the local dynamics is chaotic, there is an interval of ϵ , starting from 0.7 to 0.79, where the chaos is

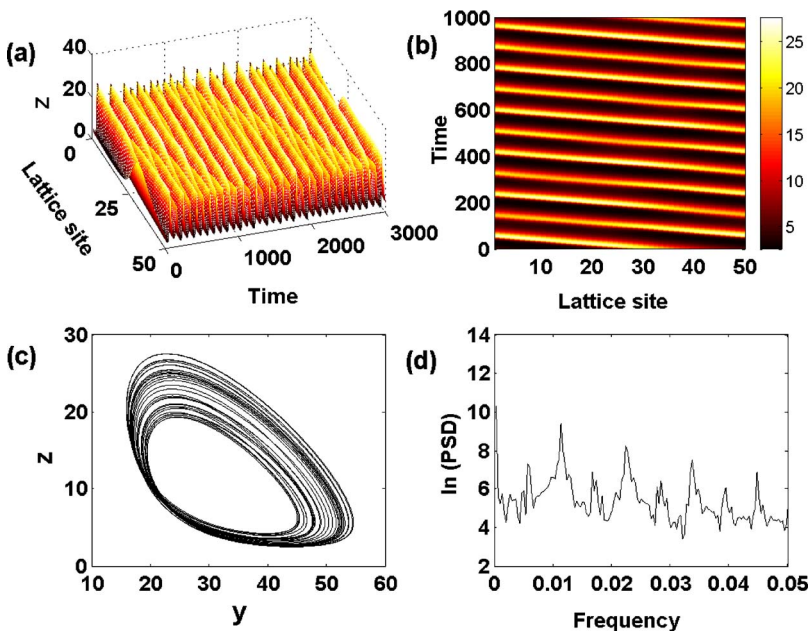


FIG. 3. (Color online) Traveling wave for $N=50$, $\epsilon=0.6$. (a) 3D space-time-concentration plot, and (b) 2D space-time plot, of z in the cells. (c) (y - z) phase portrait, and (d) power spectrum, of the 25th cell.

suppressed and the local dynamics is periodic. But as seen in Tables I and II, and Fig. 4, this feature of suppression of chaos is not sustained for higher ϵ and N . Thus, the phenomenon of synchronization in this system does not follow the usual behavior of coupled systems.

C. Quantitative study of synchronization

Synchronization is a prerequisite for coordinated collective behavior of cells, and we have shown that the coupled cell system shows different spatiotemporal dynamics with changing system size and the extent of coupling between them. To quantify the level of synchronization in the cells for the above cases we first calculate the *average synchronization error* (E) [41]. This parameter represents the extent of synchronization and its stability by calculating the temporal evolution of the spatial average of errors, i.e., the difference between the similar variables at different positions. In a coupled system, the temporal behavior of the global synchronized state will be similar to the local signals $z_i(t)$, and in the unsynchronized situation the individual signals being different from each other, their sum will be averaged out to an approximately constant value at all times.

Further, to characterize quantitatively the transition to synchronization, it is convenient to define a quantity with a value that changes abruptly at the transition point to the synchronized state, namely a *synchronization order parameter* (R). Recently an easy-to-calculate quantity [42] has been used to study synchronization in biological systems, such as, synchronization of oscillations in cell populations. Following Refs. [42], we use the ratio of the standard deviation of the time series of the average signal to the standard deviation of the individual z_i , as the *synchronization order parameter*, R . This quantity behaves as a good indicator of synchronization as it takes values close to 0 in the unsynchronized region, and close to 1 in the synchronized region, and shows a sudden change between these two limiting values when a phase transition to synchronization occurs. So, in effect, it serves as a good “order parameter” to capture the synchronization transition as it bears the signature of the transition to the synchronized state very clearly.

1. Average synchronization error

The error function E [41] is defined as

$$E(t) = (1/N) \sum_{i=1}^N \{[z_i(t) - z_{N/2}(t)]^2\}, \quad (4)$$

where the *sum of squared differences* are taken over a large time interval (10^4 time units here) after discarding transients, for calculating the average $E(t)$ ($\langle E \rangle$). When all cells in the lattice have completely synchronized dynamics, the spatial average of errors in the cells, $\langle E \rangle \approx 0$. The plot for the synchronization error E is shown in Fig. 5 for different coupling strengths and cell populations. It is clear from the plot that only small lattices show synchronization for a large range of coupling strengths, and there is no complete synchronization in the lattice for higher N for any ϵ . This is not the usual case with other systems as they tend to get synchronized for

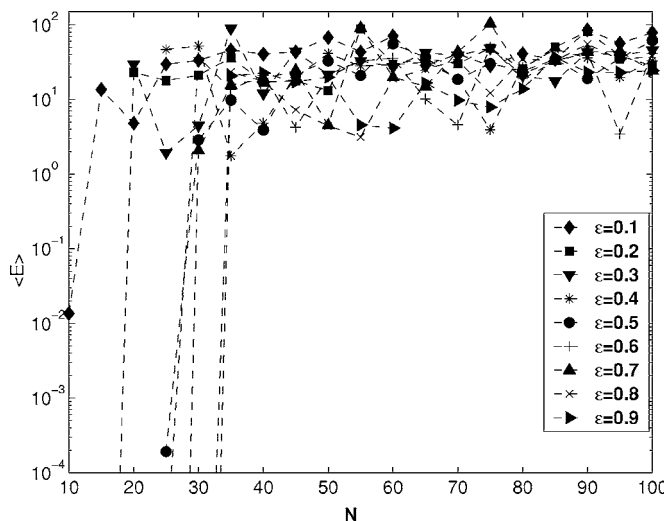


FIG. 5. Average synchronization error ($\langle E \rangle$) for different N and ϵ .

increased coupling and remain in synchronized state for higher couplings.

2. Synchronization order parameter

The synchronization order parameter R is defined to characterize quantitatively the transition to synchronization by comparing the average of the local signal to the global behavior. It is explicitly defined to be

$$\frac{\langle M^2 \rangle - \langle M \rangle^2}{[\langle z_i^2 \rangle - \langle z_i \rangle^2]}, \quad (5)$$

where the symbols $\langle \rangle$ and $[\]$ represent the temporal and spatial averaging, respectively. M is the spatial average of z over N cells at every time. This quantity has limiting values of 0 and 1. In the synchronized regime, the average state will be similar to the individual states z_i . So, $R \approx 1$ in the synchronized case. In the unsynchronized regime, the individual states will be out-of-step with respect to each other, and their sum will be averaged out to an approximately constant value at all times (exactly constant in the limit of an infinite number of completely uncorrelated cells). So $R \approx 0$ for the unsynchronized case.

Figure 6 shows the role of N and ϵ in setting up spatiotemporal order in the coupled cell lattices. Figure 6(a) plots the synchronization order parameter (R) for increasing coupling strength (ϵ) for a lattice of size $N=50$. The plot shows two interesting points. First, even though no complete synchronization ($R=1$) is observed for $N=50$ at any coupling strength, it shows a maximum $R > 0.95$ in the interval $0.66 \leq \epsilon \leq 0.82$, where the lattice shows phase synchronization with phase slip. Second, in general, the lattice shows fairly high order ($R > 0.7$) for a large range of ϵ indicating partial synchronization in IPS. Thus, in absence of complete synchronization also the coupled pathways show a high degree of order. It may be noted that, in contrast to expectation, here synchronization is not retained at higher ϵ .

Figure 6(b) shows the variation of R with the cell population size N in the lattice for $10 \leq N \leq 100$, for $\epsilon=0.72$. The

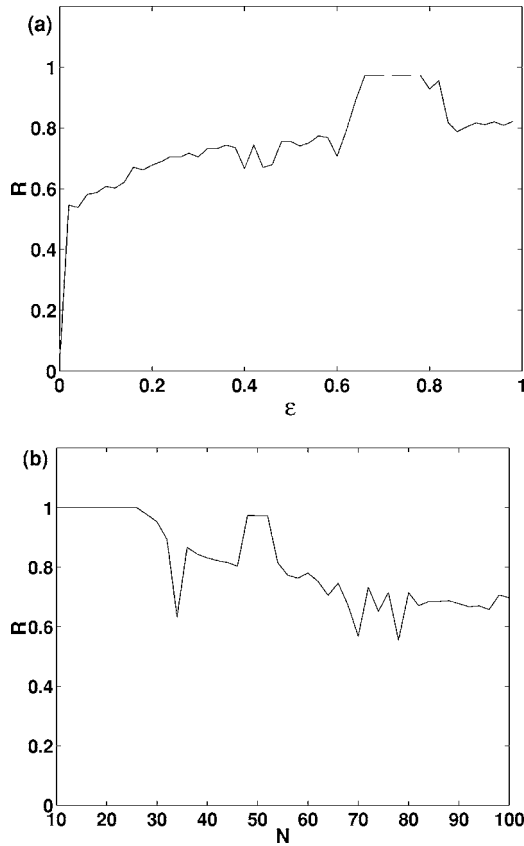


FIG. 6. Synchronization order parameter (R) with increasing (a) ϵ for $N=50$, and (b) N for $\epsilon=0.72$

coupled cell system shows complete synchrony ($R=1$) in the range $10 < N < 25$, and a local maximum of $R > 0.95$ for $48 \leq N \leq 53$, where the lattice is in the phase synchronized state. There is a general trend of decreasing R as N increases indicating intermittent phase synchronization (IPS). We have checked larger lattices (N) over a longer time interval and they continue to show intermittency.

D. Suppression of chaos and spatial pattern formation

We have shown that the inherent chaotic dynamics of the individual cells can be suppressed for a small range of metabolic coupling between the neighboring cells. In this state, both the local and global dynamics of the lattice exhibits higher periodic oscillations. Thus, the array of coupled cells forms a spatially and temporally ordered state. In this section, we discuss the spatiotemporal pattern formation in the coupled lattice when chaos is suppressed.

1. Spatial pattern formation

Figures 7(a) and 7(b) compare the long-term spatial distribution of the maxima (z_{\max}) of all cells for the uncoupled, and coupled ($\epsilon=0.72$) cells in a lattice of $N=50$ for 4000 time units. It shows the inherent chaotic dynamics of each uncoupled cell, as the peak values are distributed in an irregular manner in Fig. 7(a). A similar plot in Fig. 7(b) for the coupled cells shows regular standing wavelike spatial pattern

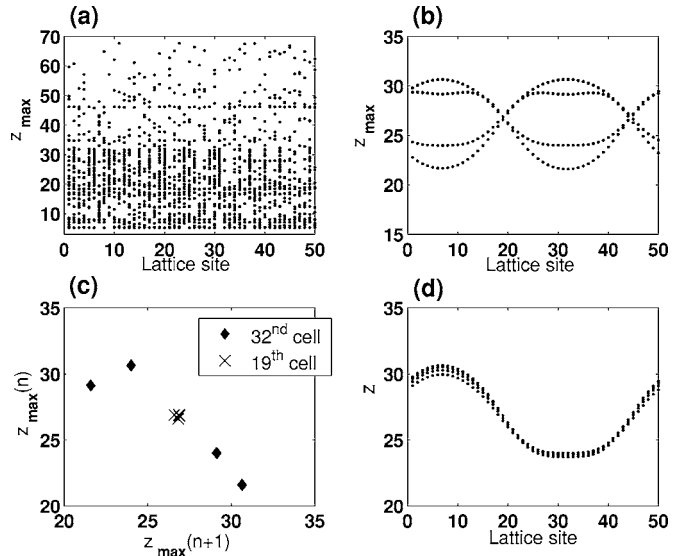


FIG. 7. Profile of the peaks of (a) uncoupled cells, (b) coupled cells showing spatial pattern; (c) return maps of a boundary cell (19th cell), and a cell at the highly variable part of the wave (32nd cell), and, (d) snapshots of the cell profiles at intervals of 365 time units. $N=50$, $\epsilon=0.72$.

in the lattice which is a horizontal “8” structure closed with two boundary points. The pattern in the periodic lattice remains constant, except for a phase shift, for any other initial condition. A closer look shows that each cell’s local dynamics corresponds to a period 4 (P4) oscillation albeit with different amplitudes. This is shown in Fig. 7(c) by the return maps of two representative cells belonging to two different parts of the wave pattern—the boundary cell (19th cell) and a cell with maximum z_{\max} (32nd cell). The boundary cells show P4 dynamics but with minimum separation of amplitude, whereas the 32nd cell shows P4 dynamics with large deviation in the maxima. All other cells have P4 dynamics with comparatively smaller deviations among the four peaks. To show that the spatial wave, once set up, repeats about every 365 time units, snapshots of the lattice were plotted every 365 time units in Fig. 7(d). This spatial pattern is indicative of standing wave where concentrations of z in some cells in space vary much more widely compared to others. Such patterns have been shown to occur in other model systems [41], and have been implicated in pattern formation in biological tissues [43].

2. Phase relationship of the cells

The phase synchronization with suppression of chaos and the spatial pattern shown by the coupled cells has important and distinct features. First, the inherent chaotic dynamics in each cell is suppressed to a lower periodic state (P4) having four local maxima of different amplitudes, which, when arranged in the descending order of heights, are ordered as (1,4,2,3). Second, there is phase entrainment with a phase slip among the cells that lead to the spatial pattern [Fig. 7(b)], and a unique global temporal pattern of “two high peaks followed by two smaller peaks” in the maxima of z [as seen in Fig. 2(g)]. To show the distribution of phases that

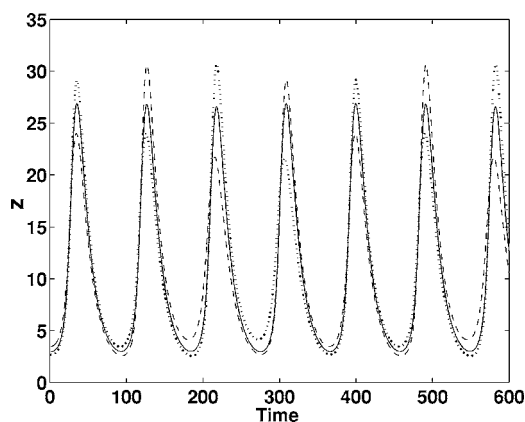


FIG. 8. Superposition of the time series showing the $T/4$ phase slip. A boundary cell (19th) in solid line, and two cells at opposite phases of the spatial wave (6th and 32nd) in dashed and dotted line, respectively. $N=50$, $\epsilon=0.72$.

underlies the spatiotemporal pattern in the lattice, we plot the time series of three cells from the lattice in Fig. 8. They are perfectly synchronized. As also seen in Fig. 7(c), the peaks of the oscillations of the boundary cell (19th in solid line) are very similar. The temporal behavior of z in two cells (6th and 32nd cells) belonging to the opposite phases of the spatial wave are shown by dashed and dotted lines. It can be seen that the two cells are phase synchronized, but the amplitude maxima are temporally arranged as (1,4,2,3) and (3,1,4,2) leading to a phase lag by one-fourth of the period of the P4 cycle due to the fixed phase slip. All cells on the two sides of the boundaries show the same phase slip. This leads to the shift of the highest peak of all the 50 cells such that the overlapped time series consists of “two high peaks followed by two smaller peaks” [as in Fig. 2(g)]. This *phase-synchronization-with-phase-slip* behavior underlies the spatiotemporal pattern in the lattice of coupled cells.

E. Consequences of random coupling among cells

Until now we have investigated the spatiotemporal dynamics of the ring of coupled cells, where the cells interact through diffusion of z only with their nearest neighbors. To introduce a small degree of randomness in spatial coupling, here we study the spatiotemporal dynamics of the same ring of cells with varying degrees of coupling connections rewired randomly in space. In our study, at every update we replace a fraction p of nearest neighbor links by connections to two other randomly chosen cells. The case of $p=0$ corresponds to the usual nearest neighbor interaction as in Eq. (3), while $p=1$ corresponds to completely random coupling [15,44,45], and is much like small world networks at low p . Note though, that unlike most studies in literature, here we *dynamically rewire* the coupling connections, namely the connections change with time, modeling a scenario where the cells have few transient random couplings. The idea here is to consider the effect of varying degrees of such coupling on the synchronization of the pathways, and determine the dynamical properties that are significantly affected by this transient randomness. To show that random rewiring has a

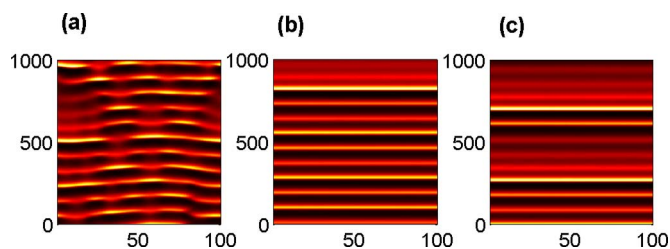


FIG. 9. (Color online) Space-time plots of the long-term evolution of z in coupled cells for rewiring fraction, (a) $p=0$, (b) $p=0.025$, and (c) $p=0.05$, for $N=100$, $\epsilon=0.7$.

pronounced and robust effect on synchronization of cellular dynamics, we present numerical results that have been obtained by sampling a large set of initial conditions, and with ring sizes ranging from 25 to 500 cells. Figure 9 displays the typical state of the evolution of the ring of size 100 for $p=0$, $p=0.025$, and $p=0.05$. Figures 10 and 11 display the synchronization error [E in Eq. (4)] and the synchronization order parameter [R in Eq. (5)], averaged over many time steps and different initial conditions, for different coupling strengths and system sizes. The figures clearly show that higher coupling strengths (ϵ) yield synchronization for smaller values of p , i.e., the transition to the synchronized state occurs for smaller degree of randomness when cells are coupled strongly. Interestingly, the transition to the synchronized state occurs at almost the same value of p for the large range of N studied. Thus, it is clear that even the smallest amount of random connections leads to complete synchronization in the coupled cell system. It is also evident from these figures that the transition to synchronization occurs at p tending to zero [45], namely the smallest degree of randomness in coupling connections yields synchronization.

The basic temporal characteristics of the randomly rewired cells are found to be the same as that of the regularly connected cells. This is evident from the similarity of the three power spectra shown in Fig. 12, for (a) $p=0$ (blue), (b) $p=0.1$ (red), and $p=0.7$ (green). The only difference is that spatially the cells are synchronized completely for the higher

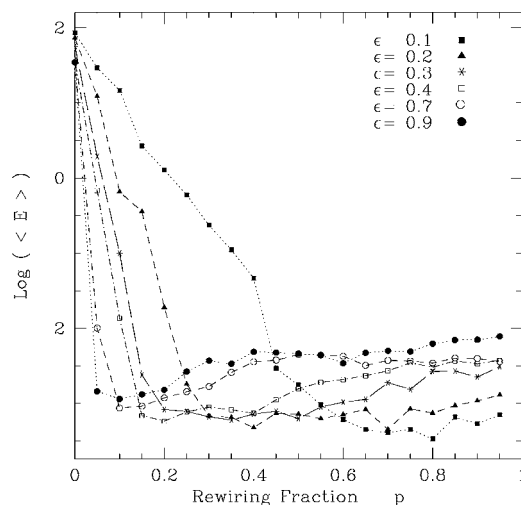


FIG. 10. The average synchronization error ($\langle E \rangle$) for different coupling strengths, with increasing rewiring fraction, p . $N=50$.

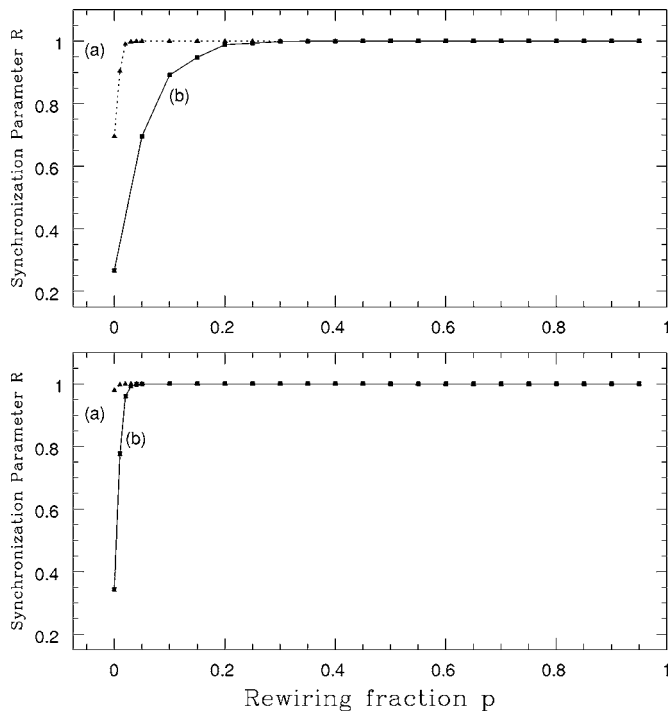


FIG. 11. The synchronization order parameter (R) with increasing rewiring fraction p . Top panel: For coupling strengths (a) $\epsilon=0.7$ and (b) $\epsilon=0.1$, for $N=50$. Bottom panel: For lattice sizes (a) $N=25$ and (b) $N=100$, for $\epsilon=0.7$.

p values. It may be mentioned however that, for quenched or static rewiring (i.e., setting a few random connections at start and not changing them from time to time), does not achieve this effect. This points to the fact that temporally transient coupling between the cells have a more pronounced effect on their mutual synchronization, than spatially fixed connections, indicating that transient connections between cells in a population induce coherence among the cells very efficiently.

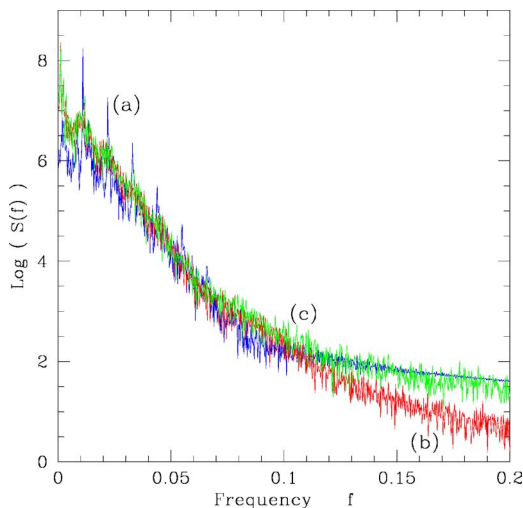


FIG. 12. (Color online) Power spectra of lattices ($N=100$ and $\epsilon=0.7$) with rewiring fraction (a) $p=0$ (blue), (b) $p=0.1$ (red), and (c) $p=0.7$ (green).

IV. DISCUSSION

Cell-to-cell communication is a crucial prerequisite for the development and maintenance of structure and function of multicellular organisms. To date, diverse mechanisms of intercellular exchange of information have been documented, and variation in strength of communication has been implicated to changes in dynamical states leading to disease [46]. Biochemical pathways with activator-inhibitor reactions underlie many cellular functions and end products of such pathways metabolically couple cells in populations and tissues for inducing collective behavior. We have investigated the collective behavior of a one dimensional ring of cells, diffusively coupled to their nearest neighbors through the end product of an intracellular activator-inhibitor biochemical pathway. The individual cells, which are chaotic when uncoupled, are found to show multiple modes of synchronized spatiotemporal dynamics—chaos suppression, phase synchronization, traveling wave, and intermittent synchronization, for ranges of coupling strength. The suppression of chaos, phase synchronization and the standing wavelike spatial pattern in this system is characterized both qualitatively and quantitatively. Unlike other systems, here synchronization does not persist for higher coupling after establishment.

Phase synchronization observed in our model has certain important and distinct features. Most of the earlier investigations [17] were concentrated on synchronization of either chaotic or limit cycle oscillators. Here, the phase entrainment is observed in a collection of oscillators whose intrinsic dynamics is a lower subharmonic state (period 4). Along with suppression of chaos to P4 oscillations, regular spatial patterns like standing waves with $T/4$ phase slips are also observed with clusters of cells in the lattice having phase synchronized dynamics but with different amplitudes. Even when the pathways in individual cells continue to exhibit chaotic dynamics, traveling waves are observed in the lattice. Traveling waves have long been shown to underlie pattern formation in tissues [47].

Quantitative analysis, using the order parameter, reveals a very interesting result. The extent of synchrony within the spatially distributed cells is not always proportional to the strength of interaction between the cells. It usually peaks at an intermediate range of coupling. Most studies of synchronization assume that a high value of synchronization index indicates a strong interaction between the component cells. Our simulations suggest that this assumption holds only for weak coupling in case of nearest neighbor interactions.

Last, we demonstrate that a small degree of randomness in the spatial coupling can lead to complete synchronization in regimes of coupling strengths which yield only intermittent synchronization for strictly nearest neighbor coupling. The robust synchronization induced by random coupling may have significant ramifications. It has immediate relevance to the important problem of synchronizing extended complex systems. Biological systems, especially cells in populations or tissues experience both internal and external noise in their natural milieu [48], and yet they show coherent activity under different conditions. Our results show that even a very small number of transient spatially random connections among the cells can lead to coherence, which

strictly nearest-neighbor coupling cannot provide. Thus, obtaining synchronization by introducing some random spatial connections, even while maintaining predominantly regular nearest neighbor contacts, suggests a natural regularizing mechanism in biological systems even in the presence of a large variation in coupling strength and lattice size. Such scenario are now being found in experimental situations

where cells can make transient random contacts with each other in an ensemble [16]. Our theoretical study is successful in providing clues that increase the general understanding of how nature engineers collective robustness in the face of local complexity.

One of the authors (S.R.) acknowledges support by the Department of Science and Technology, India.

-
- [1] A. Goldbeter and G. Nicolis, *Prog. Theor. Biol.* **4**, 65 (1976).
- [2] M. Ptashne, *A Genetic Switch* (Blackwell, Cambridge, 1992).
- [3] E. O. Voit, *Computational Analysis of Biochemical Systems* (Cambridge University Press, Cambridge, 2000).
- [4] A. Goldbeter, *Biochemical Oscillations and Cellular Rhythms* (Cambridge University Press, Cambridge, 1996).
- [5] T. Haberichter, M. Marhl, and R. Heinrich, *Biophys. Chem.* **90**, 17 (2001); G. Houart, G. Dupont, and A. Goldbeter, *Bull. Math. Biol.* **61**, 507 (1999).
- [6] G. Baier and S. Sahle, *J. Theor. Biol.* **193**, 233 (1998); K. Nielsen, P. G. Sorensen, F. Hynne, and H. G. Busse, *Biophys. Chem.* **72**, 49 (1998); I. M. De la Fuente, L. Martinez, and J. Veguillas, *BioSystems* **39**, 87 (1996).
- [7] Melissa B. Miller and Bonnie L. Bassler, *Annu. Rev. Microbiol.* **55**, 165 (2001).
- [8] M. Freeman and J. B. Gurdon, *Annu. Rev. Cell Dev. Biol.* **18**, 515 (2002).
- [9] J. W. Costerton, in *Microbial Biofilms*, edited by M. A. Ghanoun and G. O'Toole (ASM Press, Washington DC, 2004), p. 4.
- [10] Olivier Renaud and Pat Simpson, *Dev. Biol.* **240**, 361 (2001).
- [11] Catherine Lindon, Olivier Albagli, Christian Pinset, and Didier Montarras, *Dev. Biol.* **240**, 574 (2001).
- [12] J. R. Collier, N. A. M. Monk, P. K. Maini, and J. H. Lewis, *J. Theor. Biol.* **183**, 429 (1996).
- [13] P. Richard, B. Teusink, B. B. Hemker, K. van Dam, and H. V. Westerhoff, *Yeast* **12**, 731 (1996).
- [14] G. von Dassow, E. Meir, E. M. Munro, and G. M. Odell, *Nature (London)* **406**, 188 (2000).
- [15] D. J. Watts and S. Strogatz, *Nature (London)* **393**, 440 (1998); J. J. Collins and C. C. Chow, *ibid.* **393**, 409 (1998).
- [16] A. Rustom, R. Saffrich, I. Markovic, P. Walther, and H. H. Gerdes, *Science* **303**, 1007 (2004); B. Onfelt, S. Nedvetzki, K. Yanagi, and D. M. Davis, *J. Immunol.* **173**, 1511 (2004); Masamichi Koyanagi, Ralf P. Brandes, Judith Haendeler, Andreas M. Zeiher, and Stefanie Dimmeler, *Circ. Res.* **96**, 1039 (2005).
- [17] A. Pikovsky, M. Rosenblum, and J. Kurths, *Synchronization: A Universal Concept in Nonlinear Sciences* (Cambridge University Press, Cambridge, 2001).
- [18] L. M. Pecora and T. L. Carroll, *Phys. Rev. Lett.* **64**, 821 (1990); L. M. Pecora, T. L. Carroll, G. A. Johnson, D. J. Mar, and J. F. Heagy, *Chaos* **7**, 520 (1997).
- [19] M. G. Rosenblum, A. S. Pikovsky, and J. Kurths, *Phys. Rev. Lett.* **78**, 4193 (1997).
- [20] N. F. Rulkov, M. M. Sushchik, L. S. Tsimring, and H. D. I. Abarbanel, *Phys. Rev. E* **51**, 980 (1995).
- [21] M. G. Rosenblum, A. S. Pikovsky, and J. Kurths, *Phys. Rev. Lett.* **76**, 1804 (1996).
- [22] J. Y. Chen, K. W. Wong, H. Y. Zheng, and J. W. Shuai, *Phys. Rev. E* **64**, 016212 (2001).
- [23] C. Schafer, M. G. Rosenblum, H. H. Abel, and J. Kurths, *Phys. Rev. E* **60**, 857 (1999); V. V. Niulin and T. Brismar, *Neuroscience* **137**, 647 (2006); B. Blasius, A. Huppert, and Lewi Stone, *Nature (London)* **399**, 354 (1999).
- [24] A. M. Turing, *Philos. Trans. R. Soc. London, Ser. B* **227**, 37 (1952).
- [25] J. D. Murray, *Mathematical Biology* (Springer-Verlag, Berlin, 1989).
- [26] Somdatta Sinha and S. Mookerjee, *Dev. Biol.* **154**, 218 (1992).
- [27] H. Meinhardt and A. Gierer, *BioEssays* **22**, 753 (2000).
- [28] Matthew P. Harris, Scott Williamson, John F. Fallon, Hans Meinhardt, and Richard O. Prum, *Proc. Natl. Acad. Sci. U.S.A.* **102**, 11734 (2005).
- [29] C. Suguna, Kanchan K. Chowdhury, and S. Sinha, *Phys. Rev. E* **60**, 5943 (1999).
- [30] H. H. McAdams and A. P. Arkin, *Proc. Natl. Acad. Sci. U.S.A.* **94**, 814 (1997).
- [31] D. E. Koshland, Jr., A. Goldbeter, and J. B. Stock, *Science* **217**, 220 (1982); P. Smolen, D. A. Baxter, and J. H. Byrne, *Am. J. Physiol.* **274**, C531 (1998); L. Glass and M. C. Mackey, *From Clocks to Chaos: The Rhythms of Life* (Princeton University Press, Princeton, NJ, 1988); A. T. Winfree, *The Geometry of Biological Time* (Springer-Verlag, Berlin, 1980); K. Nielsen, P. G. Sorensen, F. Hynne, and H. G. Busse, *Biophys. Chem.* **72**, 49 (1998); L. F. Olsen and H. Degn, *Nature (London)* **267**, 177 (1977); B. A. Cunningham, J. T. Deeney, C. R. Bliss, B. E. Corkey, and K. Tornheim, *Am. J. Physiol.* **271**, E702 (1996); A. Malgaroli and J. Meldolesi, *FEBS Lett.* **283**, 169 (1991); H. Ishizuka, A. Hanamura, T. Inada, and H. Aiba, *EMBO J.* **13**, 3077 (1994).
- [32] S. Sinha and R. Ramaswamy, *BioSystems* **20**, 341 (1987).
- [33] B. C. Goodwin, *Analytical Physiology of Cell and Developing Organisms* (Academic, London, 1976).
- [34] J. J. Tyson, *J. Theor. Biol.* **103**, 313 (1983).
- [35] C. Suguna and Somdatta Sinha, *Fluct. Noise Lett.* **2**, L313 (2002).
- [36] *Theory and Applications of Coupled Map Lattices*, edited by K. Kaneko (Wiley, New York, 1993), and references therein.
- [37] C. Suguna and Somdatta Sinha, *Physica A* **346**, 154 (2005).
- [38] Y. Oono and S. Puri, *Phys. Rev. Lett.* **58**, 836 (1987).
- [39] F. Argoul, A. Arneodo, and P. Richetti, *Phys. Lett. A* **120**, 269 (1987); F. T. Arecchi *et al.*, *J. Opt. Soc. Am. B* **5**, 1153 (1988); M. Lefranc *et al.*, *ibid.* **8**, 239 (1991); R. Herrero, R. Pons, J. Farjas, F. Pi, and G. Orriols, *Phys. Rev. E* **53**, 5627 (1996); T. Braun, J. A. Lisboa, and J. A. C. Gallas, *Phys. Rev. Lett.* **68**,

- 2770 (1991); H. Herzel *et al.*, *Physica D* **48**, 340 (1991); M. R. Basset and J. L. Hudson, *J. Phys. Chem.* **92**, 6963 (1988).
- [40] K. Kaneko, *Phys. Rev. Lett.* **69**, 905 (1992).
- [41] N. J. Balmforth, C. Pasquero, and A. Provenzale, *Physica D* **138**, 1 (2000).
- [42] J. Garcia-Ojalvo, Michael B. Elowitz, and Steven H. Strogatz, *Proc. Natl. Acad. Sci. U.S.A.* **101**, 10955 (2004).
- [43] Seiji Takagi, Alain Pumir, Lorenz Kramer, and Valentin Krinsky, *Phys. Rev. Lett.* **90**, 124101 (2003).
- [44] S. Sinha, *Phys. Rev. E* **66**, 016209 (2002); **69**, 066209 (2004).
- [45] P. M. Gade and S. Sinha, *Phys. Rev. E* **72**, 052903 (2005).
- [46] S. Liebner, U. Cavallaro, and E. Dejana, *Arterioscler., Thromb., Vasc. Biol.* **26**, 1431 (2006); A. V. Panfilov, *Phys. Rev. Lett.* **88**, 118101 (2002); Bradford E. Peercy and James P. Keener, *SIAM J. Appl. Dyn. Syst.* **4**, 679 (2005); Claudiu A. Giurumescu, Paul W. Sternberg, and Anand R. Asthagiri, *Proc. Natl. Acad. Sci. U.S.A.* **103**, 1331 (2006).
- [47] G. C. Cruywagen, P. K. Maini, and J. D. Murray, *J. Math. Biol.* **33**, 193 (1994); S. C. Muller, T. Mair, and O. Steinbock, *Biophys. Chem.* **72**, 37 (1998).
- [48] H. H. McAdams and A. P. Arkin, *Trends Genet.* **15**, 65 (1999).